J. Fluid Mech. (2006), *vol.* 563, *pp.* 97–122.
doi:10.1017/S0022112006001066 Printed in the United Kingdom

Antisymmetric stresses in suspensions: vortex viscosity and energy dissipation

By S. FENG[1]†, A. L. GRAHAM[1], J. R. ABBOTT[2] AND H. BRENNER[3]

[1]Los Alamos National Laboratory, Los Alamos, NM 87544, USA

[2]High Performance Computing Center, Texas Tech University, Lubbock, TX 79409, USA

[3]Department of Chemical Engineering, Massachusetts Institute of Technology, Cambridge, MA 02139, USA

(Received 25 April 2005 and in revised form 2 February 2006)

When the individual particles in an otherwise quiescent suspension of freely suspended spherical particles are acted upon by external couples, the resulting suspension-scale fluid motion is characterized by a non-symmetric state of stress. Viewed at the interstitial scale (i.e. microscopic scale), this coupling between translational and rotational particle motions is a manifestation of particle–particle hydrodynamic interactions and vanishes with the volume fraction ϕ of suspended spheres. The antisymmetric portion of the stress is quantified by the suspension-scale vortex viscosity μ_v, different from the suspension's shear viscosity μ. Numerical boundary element method (BEM) simulations of such force-free suspensions of spheres uniformly dispersed in incompressible Newtonian liquids of viscosity μ_0 are performed for circumstances in which external couples (of any specified suspension-scale position-dependence) are applied individually to each of the suspended particles in order to cause them to rotate in otherwise quiescent fluids. In the absence of external forces acting on either the spheres or boundaries, such rotations indirectly, through interparticle coupling, cause translational motions of the individual spheres which, owing to the no-slip boundary condition, drag neighbouring fluid along with them. In turn, this combined particle–interstitial fluid movement is manifested as a suspension-scale velocity field, generated exclusively by the action of external couples. Use of this scheme to create suspension-scale particle-phase spin fields $\boldsymbol{\Omega}$ and concomitant velocity fields $\boldsymbol{v}$ enables both the vortex and shear viscosities of suspensions to be determined as functions of ϕ in disordered systems. This scheme is shown, *inter alia*, to confirm the constitutive equation, $\boldsymbol{T}^a = 2\mu_v \boldsymbol{\varepsilon} \cdot [(1/2)\nabla \times \boldsymbol{v} - \boldsymbol{\Omega}]$, proposed in the continuum mechanics literature for the linear relation between the antisymmetric stress $\boldsymbol{T}^a$ and the disparity existing between the particle-phase spin rate $\boldsymbol{\Omega}$ and half the suspension's vorticity, $\nabla \times \boldsymbol{v}$ (with the third-rank pseudotensor $\boldsymbol{\varepsilon}$ the permutation triadic). Our dynamically based BEM simulations confirm the previous computations of the Prosperetti *et al.* group for the dependence of the vortex viscosity upon the solids volume fraction in concentrated disordered suspensions, obtained by a rather different simulation scheme. Moreover, our dynamically based rheological calculations are confirmed by our semi-independent, energetically based, calculations that equate the rates of working (equivalently, the energy dissipation rates) at the respective interstitial and suspension scales. As an incidental by-product, the same BEM simulation results also verify the suspension-scale Newtonian constitutive equation, $\boldsymbol{T}^s = \mu[\nabla \boldsymbol{v} + (\nabla \boldsymbol{v})^\dagger]$,

† Author to whom correspondence should be addressed: sfeng@lanl.gov

as well as the functional dependence of the shear viscosity μ upon ϕ found in the literature.

1. Introduction

The vortex viscosity μ_v of suspensions of particles plays an important role in the dynamics of magnetic fluids (ferrofluids), materials of technological importance in a variety of applications-oriented and scientific contexts (Rosensweig 1997, 2003). The present paper aims, *inter alia*, to present simulation-based data for μ_v as a function of the volumetric particle concentration ϕ in homogeneous non-colloidal suspensions of monodisperse spheres. While such rheological data may not necessarily prove to be quantitatively useful in ferrofluid rheology owing to their failure to address either rotational Brownian motion (Brenner & Weissman 1972) or interparticle magnetic forces (Rosensweig 1997, 2003), their availability to researchers would nevertheless appear to represent a promising start. A secondary objective pertains to clarifying the role, if any, of couple stresses $\boldsymbol{C}$ (Condiff & Dahler 1964) in the general context of antisymmetric stresses and energetics in suspensions. Condiff & Dahler (1964) include the couple stress in the angular momentum equation as

$$\rho\kappa^2\frac{\mathrm{D}\boldsymbol{\Omega}}{\mathrm{D}t} = \nabla\cdot\boldsymbol{C} + \boldsymbol{T}_\times + \boldsymbol{G}. \tag{1.1}$$

Apart from the usual symbols appearing in (1.1), the scalar κ is the radius of gyration, while the pseudovector $\boldsymbol{\Omega}$ is the spin field. Moreover, the pseudovector $\boldsymbol{G}$ denotes the external body-couple density field (on a per unit volume basis), while $\boldsymbol{T}_\times$ denotes the pseudovector of the antisymmetric stress. However, for the reasons described in the Appendix, pertaining to the continuum aspects of (1.1), and as was independently confirmed by our BEM calculations, this couple stress contribution proves to be a vanishingly small non-continuum contribution of $O(a/L)^2$ for the class of problems addressed herein, where a is the radius of the spheres and L is the length scale on which the suspension-scale field velocity field varies. As such, the possible contribution of $\boldsymbol{C}$ to (1.1) has been explicitly eliminated from further consideration. It is also demonstrated in the Appendix that, for similar non-continuum reasons, the rotational inertial term appearing on the left-hand side of (1.1) is negligible in the present class of problems. Furthermore as discussed in the Appendix, in the absence of couple stress contributions, it is unnecessary to specify a suspension-scale spin boundary condition on solid surfaces. These conclusions allow us to focus on the μ_v vs. ϕ functional relation in a simple system that is structureless (i.e. disordered) and behaves as a continuum without the interference of couple stress, non-continuum effects, spin boundary conditions, and normal stress differences arising from the existence of microstructure in the suspensions (Gadala-Maria 1979; Drazer *et al.* 2004; Sierou & Brady 2002).

As far as we are aware, only one previous simulation scheme has explored the μ_v vs. ϕ functional relation in disordered suspensions over a significant range of particle concentrations. We refer here to the work of Prosperetti and his group (Marchioro, Tanksley & Prosperetti 2000; Marchioro *et al.* 2001; Wang & Prosperetti 2001; Ichicki & Prosperetti 2004), hereafter referred to collectively as Prosperetti *et al.*, and covering the concentration range up to $\phi = 0.5$. It will be seen that our vortex viscosity results, which cover the range up to $\phi = 0.3$, agree excellently with those of the

Prosperetti *et al.* group. Since our boundary element method (BEM) computations are based upon a different simulation scheme, such independent agreement inspires confidence in the validity of the μ_v vs. ϕ results of both groups, at least over their common range of concentrations.

Our simulation scheme differs from that of Prosperetti *et al.* In particular, their periodic Green's function simulations were performed on unbounded suspensions using spatially periodic boundary conditions extending in all three spatial directions. In contrast, our BEM simulations involved the presence of external boundaries surrounding the suspension laterally, on whose bounding surfaces conventional, physical, no-slip, fluid-mechanical boundary conditions were satisfied. Spatially periodic boundary conditions were invoked in our work only in the unbounded direction(s) parallel to these external material boundaries. This basic difference, in the light of the concordance of our results with those of the Prosperetti *et al.* group, allows us to explicitly affirm the robustness of the rheological constitutive equation governing the antisymmetric stress, as well as the reliability of the phenomenological vortex viscosity vs. particle concentration data derived from our respective simulations. Among other things, our BEM simulation scheme enabled us to clearly distinguish those contributions to the antisymmetric stress arising from the vortex viscosity μ_v appearing in the deviatoric stress tensor $\boldsymbol{T}$ from those contributions arising from the spin viscosity μ_s appearing in the couple-stress tensor $\boldsymbol{C}$ of Condiff & Dahler (1964) (cf. the Appendix). The work of Prosperetti *et al.* does not mention the subject of such couple stresses. Given the pre-eminent role assigned to couple stresses and hence to the spin viscosity in ferrofluid hydrodynamics (Rinaldi & Zahn 2002), whether warranted or not, the ability of our scheme to effect this important distinction provides a basis for regarding our work as contributing not only constitutively and phenomenologically to the subject of antisymmetric stresses, but also conceptually to the fundamental issue of couple stresses.

The trio of suspension-scale conservation equations governing the flow of incompressible suspensions composed of force-free particles are, in the absence of couple stresses (Dahler & Scriven 1961; Condiff & Dahler 1964; Brenner & Nadim 1996), respectively given by the following expressions:

(i) conservation of mass

$$\nabla \cdot \boldsymbol{v} = 0; \tag{1.2}$$

(ii) conservation of linear momentum

$$\rho \frac{\mathrm{D}\boldsymbol{v}}{\mathrm{D}t} = -\nabla p + \nabla \cdot \boldsymbol{T}^s - \tfrac{1}{2}\nabla \times \boldsymbol{T}_\times; \tag{1.3}$$

(iii) conservation of angular momentum

$$\rho\kappa^2 \frac{\mathrm{D}\boldsymbol{\Omega}}{\mathrm{D}t} = \boldsymbol{T}_\times + \boldsymbol{G}. \tag{1.4}$$

In (1.3), the deviatoric stress dyadic $\boldsymbol{T}$ has been decomposed into symmetric and antisymmetric portions,

$$\boldsymbol{T} = \boldsymbol{T}^s + \boldsymbol{T}^a, \tag{1.5}$$

in which the antisymmetric portion, $\boldsymbol{T}^a$, has been further re-expressed in terms of the pseudovector, $\boldsymbol{T}_\times$, of the antisymmetric stress via the identity,

$$\boldsymbol{T}_\times = -\boldsymbol{\varepsilon} : \boldsymbol{T}^a, \tag{1.6}$$

wherein $\boldsymbol{\varepsilon} = -\boldsymbol{I} \times \boldsymbol{I}$ is the third-order permutation pseudotriadic, in which $\boldsymbol{I}$ is the dyadic idemfactor, and wherein the double-dot notation follows the nesting convention (Dahler & Scriven 1961), rather than that of Gibbs. The inverse of (1.6) is $\boldsymbol{T}^a = (1/2)\boldsymbol{\varepsilon} \cdot \boldsymbol{T}_\times$.

The appearance of $\boldsymbol{T}_\times$ in both (1.3) and (1.4) serves to couple the respective linear and angular momentum equations. Subject to *a posteriori* verification, the suspension-scale constitutive equations governing the symmetric and antisymmetric portions of the deviatoric stress are assumed to be of the respective forms

$$\boldsymbol{T}^s = \mu[\nabla \boldsymbol{v} + (\nabla \boldsymbol{v})^\dagger] \tag{1.7}$$

and (Dahler & Scriven 1961; Condiff & Dahler 1964)

$$\boldsymbol{T}_\times = 4\mu_v\left(\tfrac{1}{2}\nabla \times \boldsymbol{v} - \boldsymbol{\Omega}\right), \tag{1.8}$$

in which μ and μ_v are, respectively, the suspension-scale shear and vortex viscosities. The spin field $\boldsymbol{\Omega}$ is implicitly understood to be the angular velocity of the particulate phase of the two-phase mixture.

The validity of (1.7) relies on the assumption of the structureless nature of the continua considered. Were the microstructure of the suspension and other non-Newtonian behaviour considered, (1.7) would be incomplete (Gadala-Maria 1979; Drazer *et al.* 2004; Sierou & Brady 2002) and it would thus be impossible for us to draw definitive conclusions pertaining to the antisymmetric stress components from this study. In the absence of external body couples and microstructure of the continuuum, the deviatoric stress tensor $\boldsymbol{T}$ would be symmetric according to the inertia-free form of (1.4). In such circumstances (1.8) shows that $\boldsymbol{\Omega} = (1/2)\nabla \times \boldsymbol{v}$, which represents a limiting condition such as exists in suspensions with random hard-sphere distributions, whereby the particulate phase spins with one-half the local vorticity $\nabla \times \boldsymbol{v}$ of the suspension (de Groot & Mazur 1962; Drazer *et al.* 2004). This state corresponds to that which occurs in conventional particle-free homogeneous fluid continua, where the spin field $\boldsymbol{\Omega}$ of the fluid continuum is imagined to be measured by the local rate of rotation of a small hypothetical unconstrained spherical particle.

The applicability of the Newtonian rheological constitutive expression (1.7) for the symmetric deviatoric stress, $\boldsymbol{T}^s$, in non-colloidal incompressible suspensions of spherical particles has been theoretically documented in the case of dilute suspensions by many, beginning with Einstein (1956) in 1905, and including Burgers (1936), Brenner (1958), Landau & Lifshitz (1959), Batchelor (1967, 1970), as well as many others. For the case of concentrated systems, numerous experiments and simulations have furnished both the shear viscosities and their respective ϕ-dependences, some values of which are later summarized in connection with figure 6. Our own BEM simulation results for the μ/μ_0 vs. ϕ relationship in concentrated disordered sphere suspensions will be seen to be generally consistent with these other data.

As regards experimental support for the validity of the constitutive expression (1.8) for the antisymmetric stress, no definitive evidence appears to exist despite its widespread use in the context of ferrofluid hydrodynamics (Rosensweig 1997, 2003). On the other hand, theoretical evidence, albeit only for dilute suspensions, does exist (Goldman, Cox & Brenner 1967; Brenner 1970*a*, *b*, 1984), although Zuzovsky, Adler & Brenner (1984) do provide some theoretical data for non-dilute ordered suspensions composed of spheres in spatially periodic arrays. While the simulation work of the Prosperetti *et al.* group might appear to substantiate the constitutive equation (1.8) in concentrated systems, it does not actually do so. Rather, assuming its validity *a priori*, their work enables one to calculate a quantity represented by the

symbol μ_v (at each and every ϕ), defined as the proportionality coefficient appearing in the relation (1.8). It does not, however, prove for the same value of ϕ that identical values of μ_v would be obtained in all physically possible rheological experiments. For example, were it to turn out, contrary to our earlier claims, that couple-stress contributions to the angular momentum equation were indeed sensible, without incorporating that possibility into the interpretation of (1.4), the verification of the constitutive equation (1.8) would not be possible.

Of course, no simulation scheme, including ours, can demonstrate the general validity of (1.8) for all of the infinitely many, experimentally possible rheological apparatus configurations. Nevertheless, by postulating the generic correctness of (1.8), it will be seen in what follows that the same μ_v/μ_0 vs. ϕ relationship (within statistically acceptable uncertainties) is obtained from our BEM simulations for at least two classes of rheological experiments, corresponding kinematically to Couette- and Poiseuille-type flows. Moreover, it will be seen, again to within statistically small uncertainties, that the functional μ_v/μ_0 vs. ϕ relationship obtained by using tensorial dynamical arguments is confirmed when employing semi-independent scalar energetic arguments. This consistency would appear to represent convincing evidence in support of the constitutive relation (1.8) as well as of the accuracy of the accompanying numerical values of the vortex viscosity. Identical arguments and commentary apply with respect to the peripheral suspension-scale shear viscosity constitutive issues in the context of (1.7).

Our twin goals of justifying the constitutive equations (1.7) and (1.8) and of calculating both the vortex and shear viscosities in non-dilute disordered suspensions are addressed herein by the use of boundary element methods. This scheme is employed to solve the detailed creeping flow equations in the interstitial fluid regions between the suspended particles and the bounding walls as well as between the suspended particles themselves, with each force-free sphere subject to an externally applied couple sufficient to collectively create suspension-scale flow in which antisymmetric stresses co-exist along with conventional symmetric stresses. We study two cases. In the first, force-free translationally mobile spheres confined between a pair of no-slip parallel plates are made to rotate with position-independent angular velocities, so as to generate a suspension-scale simple shear (Couette) flow. Similarly, in the second case, particles confined within a circular tube are made to rotate about appropriate axes with position-dependent angular velocities varying linearly with the distance of the particle from the tube axis, thereby generating a parabolic (Poiseuille) suspension-scale velocity field.

While each of these couple-animated Couette and Poiseuille flows is kinematically identical to its conventional couple-free, force-driven counterpart, whose dynamics entail only purely symmetric stresses, they nevertheless differ profoundly in their dynamic attributes from the latter, owing to the existence of antisymmetric stresses generated by the external couples applied to the particles, causing their rotations. (Differences exist not only in their respective dynamics, but also in their energetics, leading to differing energy requirements in the respective couple-animated and couple-free cases despite their kinematically identical velocity fields.) For example, whereas conventional couple-free parabolic Poiseuille flow of a homogeneous particle-free fluid in a tube at a mean velocity $\bar{V}$, say, arises from an axial pressure gradient imposed by applying an external force to the fluid as a whole, such suspension-scale pressure gradients are deliberately excluded from our external force-free, couple-driven flow, which achieves the same parabolic velocity field with mean velocity $\bar{V}$ via particle

rotation alone (although local pressure gradients will necessarily exist at the interstitial scale, albeit averaging out to a zero-mean value).

Overall, this paper consists essentially of two distinct portions, the first culminating in a dynamically based calculation of the antisymmetric stress/vortex viscosity relation, furnishing the dependence of μ_v upon ϕ. This is accomplished for both of the suspension-scale Couette- and Poiseuille-type velocity fields described above (with the subsequent, independent, BEM calculations of both data sets shown to predict essentially the same concentration dependence of the vortex viscosities). The second portion of our presentation focuses on energetic confirmation of those dynamically derived results, based upon the equality of the respective interstitial- and suspension-scale energy dissipation or, equivalently, mechanical work rates for the same overall Couette or Poiseuille kinematical flow conditions. As shown later, the dynamically derived vortex and shear viscosity results are used to calculate the suspension-scale work rate, $\dot{W}_S$, which is then compared with the corresponding interstitial-scale work rate, $\dot{W}_I$. This scheme is reminiscent of the agreement found between Einstein's (1956) original scalar energy dissipation argument calculations underlying his suspension-scale shear viscosity law, $\mu = \mu_0(1 + 2.5\phi)$, and subsequent dynamical confirmations of this relation by Burgers (1938) and others (e.g. Landau & Lifshitz 1959; Brenner 1970*a*; Cox & Brenner 1971) using tensorial stress arguments. Although the energetic and dynamical schemes used in our calculations are not wholly independent, owing to their derivation from the same set of BEM simulation data, the fact that the ratio of $\dot{W}_I$ to $\dot{W}_S$ calculated from these data is shown to be unity (within acceptable statistical uncertainties) inspires confidence in the validity of the end results, especially when viewed in the context of the agreement of our results with those of the Prosperetti *et al.* group.

Sections 2 and 3 derive the pertinent theoretical relations underlying the respective dynamical and energetic bases for interpreting the subsequent simulation data obtained by numerically solving the interstitial creeping flow equations subject to appropriate boundary conditions. Following this, in § 4, the BEM code used for these particle-level simulations is briefly described, and the resulting simulation-derived data summarized in terms of the issue of confirming (1.7) and (1.8) and of interpreting the shear and vortex viscosity vs. concentration data obtained. Section 5 reviews the main conclusions of the paper. Finally, an Appendix outlines the arguments behind our neglect of couple-stress effects.

2. Vortex viscosity

To test the validity of the proposed suspension-scale rheological constitutive equations (1.7) and (1.8), as well as to establish the respective concentration dependences of the phenomenological coefficients appearing therein, we consider, at the interstitial scale, a non-colloidal suspension of identical, net force-free, rigid spheres of radii a homogeneously dispersed in an incompressible Newtonian liquid of viscosity μ_0, with the fluid subject to appropriate interstitial-scale boundary conditions imposed at the surfaces of the individual particles and on the boundaries surrounding the suspension as a whole. In order to represent the structureless nature of the suspension, hard-sphere random distributions were employed throughout the simulations. The simulations were performed such that the force-free particles possessed both translational and angular velocities; however, the individual particle motions through space were not computed, whence possible complications arising from the formation of local microstructires were not considered. The effect of

the suspension-scale external body-couple density $\boldsymbol{G}$ was simulated, numerically, by requiring each of the individual particles ($i = 1, 2, \ldots, N$) to spin with specified angular velocities $\boldsymbol{\Omega}^i$ by the application of appropriate couples $\boldsymbol{G}^i$ to each, as detailed below. Reciprocally, the effect of the suspension-scale external body-couple density field $\boldsymbol{G}$ could also be simulated by, instead, imposing upon each of the individual particles ($i = 1, 2, \ldots, N$) specified couples $\boldsymbol{G}^i$, causing them to spin them at appropriate angular velocities $\boldsymbol{\Omega}^i$. Numerical differences between these alternative schemes were found to be negligible (Feng 2003). As a result, for brevity, the present paper focuses exclusively on use only of the former method, namely that of specifying the angular velocities $\boldsymbol{\Omega}^i$.

Each suspended sphere, being force free (so that $\boldsymbol{F}^i = \boldsymbol{0}$), necessarily translates with a velocity $\boldsymbol{U}^i$ to be determined as part of the solution scheme. Owing to the no-slip condition on the spheres, these translational particle motions drag neighbouring interstitial fluid, thereby creating a suspension-scale velocity field $\boldsymbol{v}$, representing the volume average of the local interstitial velocities together with the rigid-body velocities interior to the spheres. Use of the constitutive equations (1.7) and (1.8) in conjunction with our knowledge of $\boldsymbol{v}$ and of the suspension-scale spin field $\boldsymbol{\Omega}$ (the latter derived as discussed below from the prescribed $\boldsymbol{\Omega}^i$), enables us to calculate the suspension's respective relative vortex and shear viscosities, μ_v/μ_0 and μ/μ_0, in terms of ϕ. At the same time, our demonstration that the same values of μ_v and μ arise from independent Couette- and Poiseuille-flow BEM calculations will be seen to affirm the correctness of the constitutive equations (1.7) and (1.8) for the respective symmetric and antisymmetric stresses, in addition to offering evidence of the viability of the phenomenological viscosity data appearing therein.

The linear and angular momentum equations (1.3) and (1.4), without the inertial terms, must be solved simultaneously with the continuity equation (1.2) in order to provide suspension-scale continuum interpretations of the above interstitial-scale volume-averaged simulation results obtained for $\boldsymbol{v}$. Introduction of (1.7) and (1.8) into the inertia-free versions of (1.3) and (1.4) yields

$$-\nabla p + 2\mu_v \nabla \times \boldsymbol{\Omega} + (\mu_v + \mu)\nabla^2 \boldsymbol{v} = \boldsymbol{0} \tag{2.1}$$

and

$$2\mu_v(\nabla \times \boldsymbol{v} - 2\boldsymbol{\Omega}) + \boldsymbol{G} = \boldsymbol{0}. \tag{2.2}$$

Here, $\boldsymbol{G}$ is interpreted as being related to the individually applied external couples $\boldsymbol{G}^i$ by the expression

$$\boldsymbol{G} = \frac{1}{V}\sum_{i=1}^{N} \boldsymbol{G}^i = \frac{3\phi}{4\pi N a^3}\sum_{i=1}^{N} \boldsymbol{G}^i, \tag{2.3}$$

where a is the sphere radius and N is the number of particles present in the interstitial-scale simulation domain of volume V, which represents a periodic cell in the simulation scheme involving periodic boundary conditions imposed on the fluid boundaries of V. The above equations are further developed in the remainder of this section for the two classes of prescribed spin fields described earlier, namely position-independent in the Couette-flow scheme and linearly position-varying in the Poiseuille-flow case. The results obtained therefrom are subsequently used to calculate the suspension-scale velocity field of interest.

2.1. *Position-independent spin field; simple shear flow*

Consider a suspension bounded by a pair of no-slip parallel plates situated at $y = \pm H$ and extending indefinitely in the z-direction. At both the interstitial and suspension scales, the upper plate is taken to be force free, while the lower plate remains at rest (with all velocities subsequently being measured relative to the lower plate). The angular velocity $\boldsymbol{\Omega}^i$ of each of the suspended spheres is chosen to be

$$\boldsymbol{\Omega}^i = -\boldsymbol{\delta}_z \Omega = \text{const}, \tag{2.4}$$

where the pseudoscalar Ω is a position-independent constant, and $\boldsymbol{\delta}_z$ is a unit vector in the z-direction, pointing out of the (x, y)-plane. In conjunction with the no-slip, no-force condition, this causes the upper plate to move in the positive x-direction with velocity $U = 2\gamma H$, wherein $\gamma = U/2H$ is the suspension-scale shear rate. The subsequent BEM interstitial-scale creeping flow calculation of the velocity U of the freely moving, force-free upper plate thus ultimately serves to link the suspension-scale shear rate γ directly to: (i) the prescribed position-independent rotation rate Ω (see below) of the suspended spheres; (ii) the particle volume fraction ϕ; and (iii) the shear viscosity μ_0 of the interstitial fluid. In turn, this will be seen to enable us to calculate the suspension's relative vortex and shear viscosities, μ_v/μ_0 and μ/μ_0, as functions of ϕ.

Given that the suspension-scale pseudovector $\boldsymbol{\Omega}$ is the angular velocity of the particulate phase, and that each particle comprising that phase rotates with the same position-independent angular velocity given by the right-hand side of (2.4), it follows from the latter that the volume-average suspension-scale spin field, $\boldsymbol{\Omega} = N^{-1} \sum_i \boldsymbol{\Omega}^i$, appearing in (1.8) is given by the expression

$$\boldsymbol{\Omega} = -\boldsymbol{\delta}_z \Omega = \text{const}. \tag{2.5}$$

Subject to *a posteriori* verification, the external couple $\boldsymbol{G}^i$ required to cause the force-free sphere i to rotate with angular velocity $\boldsymbol{\Omega}^i$ is assumed to be such that

$$\boldsymbol{G}^i = -\boldsymbol{\delta}_z G^i = \text{const}. \tag{2.6}$$

Despite the constancy of Ω and the homogeneity of the suspension – the latter embodied in the relative randomness of the respective positions of the individual particles – the pseudoscalar G^i will, nevertheless, generally vary slightly in magnitude from one particle to another depending upon the instantaneous position of particle i relative to its neighbours in any given simulation. Equations (2.3) and (2.6) furnish the suspension-scale body-couple density field, $\boldsymbol{G}$.

Based upon symmetry, we further suppose, subject to *a posteriori* confirmation, that the suspension-scale velocity field is both one-dimensional and unidirectional:

$$\boldsymbol{v} = \boldsymbol{\delta}_x v(y). \tag{2.7}$$

Note that this field automatically satisfies the continuity equation (1.2). The boundary conditions $v(H) = U = 2\gamma H$ and $v(-H) = 0$ lead, of course, to the simple shear flow

$$v(y) = \gamma(y + H). \tag{2.8}$$

To relate the constant γ to the particle spin rate Ω, we note as a consequence of (2.6)–(2.8), together with use of the constitutive equations for the symmetrric and antisymmetric stresses, that (1.5) adopts the form

$$\boldsymbol{T} = (\boldsymbol{\delta}_x \boldsymbol{\delta}_y + \boldsymbol{\delta}_y \boldsymbol{\delta}_x)\mu\gamma + (\boldsymbol{\delta}_x \boldsymbol{\delta}_y - \boldsymbol{\delta}_y \boldsymbol{\delta}_x)\mu_v(2\Omega - \gamma). \tag{2.9}$$

Obviously, in circumstances where $\Omega = \gamma/2$, such as would occur in the absence of couples restraining the particles from rotating freely in a simple shear flow, there would be no antisymmetric stress.

Subject to *a posteriori* verification, the suspension-scale pressure is assumed to be constant throughout the suspension, whence we may take it to be zero without loss of generality:

$$p = 0. \tag{2.10}$$

Accordingly, the suspension's pressure tensor,

$$\boldsymbol{\Pi} = -\boldsymbol{I}p + \boldsymbol{T}, \tag{2.11}$$

is identical to its deviatoric stress (2.9) in the present case.

The force $\mathrm{d}\boldsymbol{F}$ acting on a directed surface element $\mathrm{d}\boldsymbol{S} = \boldsymbol{\delta}_y \,\mathrm{d}x\,\mathrm{d}z$ lying on a plane $y = \text{const}$ is given by the expression $\mathrm{d}\boldsymbol{F} = \mathrm{d}\boldsymbol{S}\cdot\boldsymbol{\Pi}$. As such, the condition that the top surface, $y = H$, be force free requires that $\boldsymbol{\delta}_y \cdot \boldsymbol{T} = 0$ on that surface. From (2.9) this boundary condition necessitates that $\mu\gamma - \mu_v(2\Omega - \gamma) = 0$. Equivalently,

$$\gamma = 2\Omega \frac{\mu_v}{\mu + \mu_v}. \tag{2.12}$$

Consequently, it follows from (2.9) that the stress tensor is the position-independent constant

$$\boldsymbol{T} = \boldsymbol{\delta}_x \boldsymbol{\delta}_y 4\Omega \frac{\mu\mu_v}{\mu + \mu_v} = \text{const}. \tag{2.13}$$

Note that (2.5), (2.8) and (2.10) together with the preceding constancy of the deviatoric stress confirms that the linear momentum equation (1.3) is indeed satisfied, with the pressure being constant throughout the suspension, as in (2.10). As such, our *a posteriori* assumptions are seen to be internally consistent.

It follows from (2.13) that

$$\boldsymbol{T}_\times = \boldsymbol{\delta}_z 4\Omega \frac{\mu\mu_v}{\mu + \mu_v}. \tag{2.14}$$

Alternatively, upon using (2.12) to eliminate μ from this relation, this makes $\boldsymbol{T}_\times = \boldsymbol{\delta}_z 2\mu_v(2\Omega - \gamma) = \text{ const}$. This, in conjunction with (1.4) from which the inertial terms have been eliminated, gives, upon use of (2.3) and (2.6),

$$\mu_v = \frac{3\phi\bar{G}}{16\pi a^3(\Omega - \gamma/2)}, \tag{2.15}$$

where

$$\bar{G} = \frac{1}{N}\sum_{i=1}^{N} G^i \tag{2.16}$$

denotes the magnitude of the couple exerted on an average particle in the suspension required to cause a particle to rotate with the specified angular velocity Ω. Similarly to $\bar{G}$, the effective shear rate γ appearing in (2.15), together jointly governing the value obtained for μ_v, would be expected to show small variations from one simulation to the next.

Operationally, (2.15) enables the vortex viscosity to be calculated from our subsequent interstitial BEM calculations, since these calculations furnish both $\bar{G}$ and γ for a specified Ω. As a by-product, the relation

$$\mu = \mu_v \left(\frac{2\Omega}{\gamma} - 1\right) \tag{2.17}$$

derived from (2.12) enables the shear viscosity μ to be calculated from these same simulation data.

2.2. *Linearly varying spin field; parabolic flow*

This subsection furnishes the suspension-scale equations describing flow within a circular cylindrical tube of radius R whose force-free particles spin at rates linearly proportional to their respective distances r_i from the cylinder's z-axis (and about space-fixed axes to be described). No-slip boundary conditions are applied along the tube wall, which is at rest (with all velocities subsequently being measured relative to this wall), and on the particle surfaces. A position-independent suspension-scale pressure gradient, $P = -\mathrm{d}p/\mathrm{d}z$, is also temporarily incorporated into the analysis in order to compare the flow generated by applying particle couples with the conventional Poiseuille flow generated by an axial pressure gradient. However, our main goal is to focus on the flow created exclusively by particle rotation in the absence of externally applied forces, for which $P = 0$. Thus, our temporary inclusion of a non-zero P merely serves as a frame of reference for what is follow. Ultimately, our BEM calculations are based exclusively upon the case $P = 0$.

With $(\boldsymbol{\delta}_r, \boldsymbol{\delta}_\theta, \boldsymbol{\delta}_z)$ a right-handed system of unit vectors in the circular cylindrical coordinate system (r, θ, z), the angular velocity of each suspended sphere ($i = 1, 2, \ldots, N$) relative to the tube walls is chosen to be

$$\boldsymbol{\Omega}^i = \boldsymbol{\delta}_\theta{}^i \Omega r_i / R, \tag{2.18}$$

with Ω a position-independent constant having the dimensions of a spin rate and $\boldsymbol{\delta}_\theta{}^i$ the tangential unit vector passing through the centre (r_i, θ_i, z_i) of sphere i. Subject to *a posteriori* verification, we thus suppose that the suspension-scale spin field is given by the expression

$$\boldsymbol{\Omega} = \boldsymbol{\delta}_\theta \Omega r / R. \tag{2.19}$$

We further suppose, subject to the same caveat, that the external couple required to cause the ith particle to rotate with the angular velocity given by (2.18) is

$$\boldsymbol{G}^i = \boldsymbol{\delta}_\theta{}^i G^i r_i / R, \tag{2.20}$$

where, as was true of the comparable quantity appearing in the preceding simple shear flow analysis, during any given simulation the scalar G^i appearing above is expected to depend weakly upon the radial location r_i of particle i. Based upon symmetry, we further suppose, again subject to subsequent confirmation, that at the suspension scale, $\boldsymbol{v} = \boldsymbol{\delta}_z v(r)$, which automatically satisfies the continuity equation (1.2).

Equations (2.1) and (2.2) are readily solved subject to the following trio of requirements: (i) $P =$ const; (ii) $v = 0$ at $r = R$; and (iii) v is finite at $r = 0$. This yields the Poiseuille-like parabolic velocity field

$$\boldsymbol{v} = \boldsymbol{\delta}_z 2\bar{V}[1 - (r/R)^2], \qquad p = -Pz + \text{const}, \tag{2.21}$$

in which $\bar{V}$ is the mean velocity of flow through the tube, which related to the pressure gradient by the expression

$$P = \frac{4}{R}\left[\mu \frac{2\bar{V}}{R} - \mu_v \left(\Omega - \frac{2\bar{V}}{R}\right)\right]. \tag{2.22}$$

Incidental results related to the present calculation are as follows:

$$\boldsymbol{T} = \boldsymbol{\delta}_r \boldsymbol{\delta}_z \frac{2r}{R}\left[\mu_v \left(\Omega - \frac{2\bar{V}}{R}\right) - \mu \frac{2\bar{V}}{R}\right] - \boldsymbol{\delta}_z \boldsymbol{\delta}_r \frac{2r}{R}\left[\mu_v \left(\Omega - \frac{2\bar{V}}{R}\right) + \mu \frac{2\bar{V}}{R}\right] \tag{2.23}$$

and

$$\boldsymbol{T}_{\times} = -\boldsymbol{\delta}_{\theta}\frac{4\mu_v r}{R}\left(\Omega - \frac{2\bar{V}}{R}\right). \tag{2.24}$$

The deviatoric stress (2.23) satisfies the linear momentum equation (1.3), re-written in the form $\boldsymbol{\delta}_z P + \nabla\cdot\boldsymbol{T} = \boldsymbol{0}$, which is equivalent to the relation $\nabla\cdot\boldsymbol{\Pi} = \boldsymbol{0}$, with the pressure tensor defined in (2.11).

Several things are noteworthy about this Poiseuille-flow solution. First, $\Omega = 2\bar{V}/R$ when the particle phase rotates freely with half the local vorticity of the fluid phase, as in the case of conventional Poiseuille flow. In such circumstances it follows from either (2.24) or (2.23) that the antisymmetric stress vanishes, and that the pressure gradient (2.22) reduces to the conventional Poiseuille's law relation, $P = 8\mu\bar{V}/R^2$. On the other hand, as earlier discussed, we are interested in the case where there is no suspension-scale pressure gradient, i.e. $P = 0$. In that case it follows from (2.22) that the mean velocity through the cylinder, generated exclusively by rotation of the spheres, is

$$\bar{V} = \frac{1}{2}\Omega R\frac{\mu_v}{\mu + \mu_v}, \tag{2.25}$$

which represents the analogue of the Couette-flow relation, (2.12). With the use of the above expression, (2.24) in conjunction with the relation $\boldsymbol{T}_x + \boldsymbol{G} = \boldsymbol{0}$ gives, for the local body-couple density at a point of the suspension,

$$\boldsymbol{G} = \boldsymbol{\delta}_{\theta}\frac{4\mu\mu_v\Omega r}{(\mu + \mu_v)R}. \tag{2.26}$$

In addition, (2.23) becomes

$$\boldsymbol{T} = -\boldsymbol{\delta}_z\boldsymbol{\delta}_r\frac{4\mu\mu_v\Omega r}{(\mu + \mu_v)R}, \tag{2.27}$$

analogous to (2.13). In regard to forces and couples in the present $P = 0$ case, we note from (2.27) that, among other things, no traction exists at any point on the tube walls, since with $\mathrm{d}\boldsymbol{S}_r = \boldsymbol{\delta}_r R\,\mathrm{d}\theta\,\mathrm{d}z$ a directed element of surface area on the walls, $r = R$, it follows that $\mathrm{d}\boldsymbol{S}_r\cdot\boldsymbol{\Pi} = \boldsymbol{0}$. Thus, remarkably, despite the usual velocity gradient existing at the no-slip walls of the parabolic flow field, (2.21) (with $P = 0$), there is no force or normal stress at any point on the walls. On the other hand, on the two end caps of the cylinder, whereon $\mathrm{d}\boldsymbol{S}_z = \pm\boldsymbol{\delta}_z r\,\mathrm{d}r\,\mathrm{d}\theta$, there is, locally, at each point thereon a non-zero force, $\mathrm{d}\boldsymbol{S}_z\cdot\boldsymbol{\Pi} \neq \boldsymbol{0}$. Since, however, $\int_0^{2\pi}\boldsymbol{\delta}_r\,\mathrm{d}\theta = \boldsymbol{0}$, no net force acts on either end. (We note parenthetically that despite the existence of the local body-couple density field, $\boldsymbol{G}$, the total couple exerted upon the contents of the suspension as a whole is zero, since $\int_V \boldsymbol{G}\,\mathrm{d}V$ (with $\mathrm{d}V = r\mathrm{d}r\,\mathrm{d}\theta\,\mathrm{d}z$ a volume element) integrates to zero. While this is true for the present case of Poiseuille flow in a tube, it would not be true, say, for the comparable case of two-dimensional Poiseuille flow between flat plates, where the axes of rotation of the spheres would all lie in the z-direction, perpendicular to the (x, y) net-flow plane.)

With regard to use of the preceding suspension-scale Poiseuille formulas in interpreting our subsequent BEM simulation calculations, we note that use of (2.2) together with (2.3), (2.20) and (2.24) gives

$$\mu_v = \frac{3\phi\bar{G}}{16\pi a^3(\Omega - 2\bar{V}/R)}, \tag{2.28}$$

where

$$\bar{G} = \frac{1}{N}\sum_{i=1}^{N}\left(\frac{r_i}{r}\right)G^i \tag{2.29}$$

denotes the average value of the weakly varying quantity G^i. Were G^i in the subsequent simulations indeed found to be sensibly independent of the position of r_i, at least to the extent that r_i/r could, in effect, be removed from beneath the summation sign without significant error, it would then follow (from the fact that $\sum_{i=1}^{N}(r_i/r)=N$, at least statistically in our disordered suspensions), that $\bar{G}$ would be equal to G^i. Of course, this position-independence of G^i will not prove to be exactly true, with the degree of departure from constancy depending upon the position of sphere i relative to its neighbours in any given simulation of the randomly ordered particle arrangement. As such, from a computational point of view, all other things being equal, small variations in the value of $\bar{G}$ will occur from one simulation to the next. Similarly, the quantity $\bar{V}$, obtained by appropriately volume averaging the interstitial-scale creeping flow velocity, $\boldsymbol{v}(r,\theta,z)$, would be expected to show small variations from one simulation to the next, analogous to those discussed in the simple shear case.

Similarly to (2.17), on the basis of (2.25) rewritten as

$$\mu=\mu_v\left(\frac{\Omega R}{2\bar{V}}-1\right), \tag{2.30}$$

one can obtain numerical values of the shear viscosity from the same parabolic flow simulation data as were used to calculate the vortex viscosity.

3. Energy dissipation

Energetically speaking, in the case of incompressible inertia-free linear and angular momentum transport, all of the work being done by the external couples exerted upon the fluid is dissipated. In steady-state isothermal systems this is manifested by the conversion of work into heat, which flows out of the system into the surroundings. With $\dot{W}_S$ the temporal rate at which suspension-scale work is being done on the contents of a domain of volume V, we have in the absence of external body forces and couple stresses, but in the presence of external body couples, that (Brenner & Nadim 1996; Rinaldi & Brenner 2002) $\dot{W}_S=\oint_{\partial V}\mathrm{d}\boldsymbol{S}\cdot\boldsymbol{\Pi}\cdot\boldsymbol{v}+\int_V\boldsymbol{G}\cdot\boldsymbol{\Omega}\,\mathrm{d}V$, with ∂V the closed surface bounding V. Use of the fact that $\nabla\cdot\boldsymbol{\Pi}=\boldsymbol{0}$ and $\nabla\cdot\boldsymbol{v}=0$ together with (1.5) and some obvious identities leads eventually to the relation

$$\dot{W}_S=\int_V\boldsymbol{T}^s\!:(\nabla\boldsymbol{v})^s\,\mathrm{d}V+\int_V\boldsymbol{T}^a\!:(\nabla\boldsymbol{v})^a\,\mathrm{d}V+\int_V\boldsymbol{G}\cdot\boldsymbol{\Omega}\,\mathrm{d}V,$$

where the superscripts s and a refer to the respective symmetric and antisymmetric portions of the dyadic to which they are affixed. The integrand of the second term can be re-expressed as $\boldsymbol{T}^a\!:(\nabla\boldsymbol{v})^a=(1/2)\boldsymbol{T}_\times\cdot(\nabla\times\boldsymbol{v})$. Together with the inertia-free form of (1.3), we thus obtain

$$\dot{W}_S=\tfrac{1}{2}\int_V\boldsymbol{T}^s\!:[\nabla\boldsymbol{v}+(\nabla\boldsymbol{v})^\dagger]\,\mathrm{d}V+\int_V\boldsymbol{T}_\times\cdot\left[\tfrac{1}{2}(\nabla\times\boldsymbol{v})-\boldsymbol{\Omega}\right]\mathrm{d}V.$$

Finally, this when combined with the suspension-scale constitutive equations (1.7) is and (1.8) gives

$$\dot{W}_S=\frac{1}{2\mu}\int_V\boldsymbol{T}^s\!:\boldsymbol{T}^s\,\mathrm{d}V+\frac{1}{4\mu_v}\int_V\boldsymbol{T}_\times\cdot\boldsymbol{T}_\times\,\mathrm{d}V \tag{3.1}$$

for the suspension-scale rate of working, $\dot{W}_S$ (Feng 2003). The corresponding interstitial-scale work rate effected by the couples acting upon the individual spheres,

say $\dot{W}_I$, is, in the present case, where no work is done either at the material boundaries or at the ends of the domain V (Feng 2003),

$$\dot{W}_I = \sum_{i=1}^{N} \boldsymbol{G}^i \cdot \boldsymbol{\Omega}^i. \tag{3.2}$$

This is, of course, the interstitial-scale analogue of the suspension-scale relation $\dot{W}_S = \int_V \boldsymbol{G} \cdot \boldsymbol{\Omega}\, \mathrm{d}V$ from which (3.1) was derived

In the simple shear flow case treated in § 2.1, it follows upon introducing (2.9) into (3.1) that

$$\frac{\dot{W}_S}{V} = \mu\gamma^2 \left[1 + \frac{\mu_v}{\mu}\left(\frac{2\Omega}{\gamma} - 1\right)^2\right], \tag{3.3}$$

where $V = \int_V \mathrm{d}V$ is the volume of the domain. Equation (2.17) may be used to eliminate either μ or μ_v from this expression, so as to express the work rate entirely in terms of either one of these two suspension-scale viscosities. Equation (3.3) shows, as was to be expected, that in circumstances where the spin rate matches half the suspension-scale vorticity, corresponding to the situation where $\Omega = \gamma/2$, no dissipation ensues from the spin since this circumstance corresponds to the case where the suspended particles rotate freely, unconstrained by the action of couples. Were this to be the case, for a given shear rate γ, albeit now furnished by applying forces to the plates rather than by applying couples to the particles, the rate of working per unit volume would be $\mu\gamma^2$. Thus, all other things being equal, if $\dot{w}_G$ and $\dot{w}_F$ represent the rates of working per unit volume required to achieve a given shear rate γ by respectively applying couples to the spheres or forces to the plates, one has upon using (2.12) that

$$\frac{\dot{w}_G}{\dot{w}_F} = 1 + \frac{\mu}{\mu_v}. \tag{3.4}$$

As this work-rate ratio is greater than unity, applying couples to create a specified simple shear flow at rate γ is clearly less energy efficient than applying forces. By way of example, in dilute systems (Brenner 1970*a*, *b*), where $\mu_v/\mu_0 \to 1.5\phi$ as $\phi \to 0$, equation (3.4) asymptotes to $\dot{w}_G/\dot{w}_F \to 0.667/\phi$, thus becoming extremely large at low particle concentrations.

In the parabolic flow case treated in § 2.2, where the volume element for a length L of tube is $\mathrm{d}V = 2\pi L r\, \mathrm{d}r$, one finds from (2.23) upon performing the requisite integration of (3.1) that

$$\frac{\dot{W}_S}{V} = \frac{8\mu\bar{V}^2}{R^2}\left[1 + \frac{\mu_v}{\mu}\left(\frac{\Omega R}{2\bar{V}} - 1\right)^2\right]. \tag{3.5}$$

Analogously to the preceding simple shear case, (2.30) may be used to eliminate either μ or μ_v from this expression. Moreover, when the particles rotate freely, corresponding to $\Omega = 2\bar{V}/R$, there is again no dissipation resulting from the spin. This freely rotating sphere case corresponds to the classical situation of a purely pressure-driven Poiseuille flow animated by the application of external forces, for which the rate of working per unit volume of duct, say $\dot{w}_F$, is given by the expression $\dot{w}_F = 8\mu\bar{V}^2/R^2$. On the other hand, in the absence of an externally imposed pressure gradient P, where the mean flow $\bar{V}$ is driven exclusively by the particle rotations, and for which case Ω is related to $\bar{V}$ by (2.25), it follows from (3.5) that the corresponding per-unit-volume

couple-driven work rate, say $\dot{w}_G$, is $\dot{w}_G = 8\bar{V}^2\mu[1 + (\mu/\mu_v)]$. For a given flow rate $\bar{V}$ it thus follows upon use of (2.25) that

$$\frac{\dot{w}_G}{\dot{w}_F} = 1 + \frac{\mu}{\mu_v}. \tag{3.6}$$

Again, as in the previous simple shear flow case, couple-driven flow is seen to be less energy efficient than is its force-driven counterpart.

As the suspension-scale velocity field is presumably accurately simulated by its volume-averaged interstitial velocity counterpart, it follows in the simple shear flow case for specified rotation and shear rates, Ω and γ, common to both scales of description, that the respective rates of working must be the same in order that the laws of thermodynamics be obeyed independently of the scale at which the phenomenon is being viewed. As such, by equating $\dot{W}_I$ to $\dot{W}_S$, it should be possible to calculate both μ_v and μ via this energetic scale-invariance scheme. In turn, the values of μ_v and μ derived by this energetic scheme should be identical to those derived by the dynamical scheme outlined in § 2. Reciprocally, the ratio of $\dot{W}_S$ (calculated by using the dynamically derived μ_v and μ values) to $\dot{W}_I$ should be unity, at least to within the accuracy of the calculations. This will be seen to be the case (cf. figure 7). Of course, since the same simulation data set is used in both schemes, the respective dynamic and energetic calculations cannot be regarded as wholly independent. Nevertheless, such internal consistency should inspire confidence in the final conclusions regarding the validity of the constitutive equations (1.7) and (1.8), as well as in the values obtained for the respective vortex and shear viscosities. These arguments apply, of course, to both the Couette- and Poiseuille-flow cases.

4. Numerical simulation

4.1. *Boundary blement method overview*

BEM simulations (Brebbia, Telles & Wrobel 1984) were used in this study to model the creeping flow of suspensions of uniform, force-free spheres randomly dispersed in Newtonian liquids and subjected to couples chosen so as to cause each sphere to rotate with a predetermined angular velocity. A detailed description of the general BEM scheme can be found elsewhere (Ingber 1989; Mondy, Ingber & Dingman 1991; Dingman 1992). The basic feature of the method is that the (closed) domain of interest, V, needs to be discretized into elements only on its boundaries, ∂V. Explicitly, the BEM scheme is such that the requisite numerical solution of the differential equations governing the particular problem posed, and satisfying prescribed boundary conditions, can ultimately be obtained throughout the entire domain by the expedient of initially having to solve for the pertinent unknowns or parameters (e.g. velocity or stress) only on the domain's boundaries. Since no nodes exist in the interior of the domain during this portion of the overall calculation, the number of unknowns that need to be solved for simultaneously is significantly reduced compared to the number required in other solution schemes. Having established the values of the nodal parameters on the boundaries, the solution throughout the domain's interior can then be achieved by using the differential equations governing the phenomena to derive simple algebraic expressions relating the respective values of the parameters at the interior nodes to those at the boundaries.

Until otherwise stated, all equations and symbols appearing below in this section refer to interstitial-level fields. At each point in the interstices, incompressible

quasi-static Stokes flow obeys the following differential equations:

$$\nabla \cdot \boldsymbol{v} = 0, \tag{4.1}$$

$$\nabla \cdot \boldsymbol{\Pi} = \boldsymbol{0}, \tag{4.2}$$

with $\boldsymbol{\Pi}$ the interstitial pressure tensor,

$$\boldsymbol{\Pi} = -\boldsymbol{I}p + \mu_0[\nabla \boldsymbol{v} + (\nabla \boldsymbol{v})^{\dagger}]. \tag{4.3}$$

The boundaries ∂V of the fluid domain V can be decomposed as follows:

$$S = S^f + \sum_{i=1}^{N} S^i, \tag{4.4}$$

where S^f represents the fixed boundaries of V, and S^i the surface of the ith particle.

Equations (4.1)–(4.3) can be cast into integral form by using a weighted residual form of these equations with weighting functions given by the fundamental solution of the Stokes equations. In Cartesian tensor notation, the Stokes velocity field v_k at a point $\boldsymbol{x}$ of the fluid which is generated by the presence of a point force of strength F_l situated at $\boldsymbol{y}$ is given by the expression $v_k = v^{\star}_{kl} F_l$, wherein (cf. Mondy *et al.* 1991; Kim & Karrila 1991)

$$v^{\star}_{kl}(\boldsymbol{x}, \boldsymbol{y}) = \frac{1}{8\mu_0 \pi r}(\delta_{kl} + r_{,k} r_{,l}), \tag{4.5}$$

in which δ_{kl} is the Kronecker function and $\boldsymbol{r} = \boldsymbol{x} - \boldsymbol{y}$ is the vector displacement between the field point $\boldsymbol{x}$ and the source point $\boldsymbol{y}$. Moreover, $r = |\boldsymbol{r}|$ is the separation between these two points.

The resulting boundary integral equation (BIE), obtained by use of the Lorentz reciprocal theorem (Happel & Brenner 1965), is

$$c_{lj}(\boldsymbol{x}) v_j(\boldsymbol{x}) + \int_S q^{\star}_{jkl}(\boldsymbol{x}, \boldsymbol{y}) v_k(\boldsymbol{y}) n_j(\boldsymbol{y}) \, \mathrm{d}S = -\int_S v^{\star}_{lj}(\boldsymbol{x}, \boldsymbol{y}) t_j(\boldsymbol{y}) \, \mathrm{d}S, \tag{4.6}$$

where $\boldsymbol{t} = \boldsymbol{n} \cdot \boldsymbol{\Pi}$ is the traction along the surface S, $\boldsymbol{n}$ is the unit outward normal vector to the boundary S, and

$$q^{\star}_{jkl}(\boldsymbol{x}, \boldsymbol{y}) = -\frac{3}{4\pi} \frac{r_{,j} r_{,k} r_{,l}}{r^2}. \tag{4.7}$$

The coefficient tensor c_{lj} can be determined from the geometry or by integrating $q^{\star}_{jkl}$ over S (Dingman 1992).

Owing to the no-slip boundary condition, the velocity at a point $\boldsymbol{x}$ on the surface of sphere i can be related to the sphere's angular velocity $\boldsymbol{\Omega}^i$ and to the velocity $\boldsymbol{U}^i$ at the centre $\boldsymbol{x}^i$ of the sphere by the expression

$$\boldsymbol{v} = \boldsymbol{U}^i + \boldsymbol{\Omega}^i \times (\boldsymbol{x} - \boldsymbol{x}^i) \text{ on } S^i. \tag{4.8}$$

The surface S^i of each of the spheres is discretized into N_E triangular and quadrilateral boundary elements. For the super-parametric treatment used in this study, the velocities and stresses are assumed constant within each element, whereas quadratic shape (Dingman 1992) functions are used to define the surface geometry. The

discretized equation for the nth element takes the following form:

$$c_{lj}^{(n)}(\boldsymbol{x})v_j^{(n)}(\boldsymbol{x}) + \sum_{(n)=1}^{N_E} \int_{(n)} N^{(n)}(\boldsymbol{y}) q_{jkl}^{\star}(\boldsymbol{x}, \boldsymbol{y}) v_k^{(n)}(\boldsymbol{y}) n_j^{(n)}(\boldsymbol{y}) \, \mathrm{d}S^{(n)}$$

$$= -\sum_{(n)=1}^{N_E} \int_{(n)} N^{(n)}(\boldsymbol{y}) v_{lj}^{\star}(\boldsymbol{x}, \boldsymbol{y}) t_j^{(n)}(\boldsymbol{y}) \, \mathrm{d}S^{(n)}. \quad (4.9)$$

The superscript (n) appearing above refers to the value on the nth element of the quantity to which it is affixed whereas $N^{(n)}(\boldsymbol{y})$ is the shape function, while N_E represents the total number of elements lying on all of the surfaces of the spheres.

The resulting algebraic system of equations is closed by enforcing the specified force $\boldsymbol{F}^i$ and couple $\boldsymbol{G}^i$ on each of the spheres. Explicitly, for each sphere S^i in the suspension we require that

$$\int_{S^i} \boldsymbol{t} \, \mathrm{d}S = \boldsymbol{0}, \quad (4.10)$$

$$\int_{S^i} (\boldsymbol{x} - \boldsymbol{x}^i) \times \boldsymbol{t} \, \mathrm{d}S + \boldsymbol{G}^i = \boldsymbol{0}. \quad (4.11)$$

In this scheme the fundamental singular solutions of the governing differential equations are continuously distributed over the boundaries of the system, whence the preceding boundary conditions lead to integral equations for the density distributions of these fundamental solutions. In addition to reducing the dimensionality of the problem posed, the method is particularly attractive in the case of Stokes-flow problems, since it represents a very general approach, independent of the body geometry as well as the form of the external flow field (Dingman 1992). A closed-form solution of the resulting integral equation is, in general, not possible, thus requiring a numerical solution.

4.2. *Numerical experiments and results*

The simulations were carried out using a BEM code (Dingman 1992) developed with the numerical algorithm described in the preceding subsection. The three-dimensional element meshes for the spheres and cylindrical container used in the Poiseuille-flow case are shown in figure 1, which depicts a periodic cell of radius R and length $4R$ containing 160 spheres. Not shown is the comparable figure for the Couette-flow case involving a cube of side $2H$, also containing 160 spheres. In order to simulate the unboundedness of the suspension in one or more directions, where required, periodic boundary conditions were applied, namely in the x- and z-directions in the parallel plate case, and in the z-direction in the circular tube case. In each case the spheres were placed randomly in the bounded cell, and the results for that particular configuration determined. The suspension-scale properties for each concentration ϕ were eventually obtained by averaging 30 such configurations. Spot-checking the results by use of a two-sided Student t-test (Johnson 1965) showed that no statistical difference existed between any two sets of the 30-configuration average. (Where shown explicitly on subsequent figures, the indicated error bars were calculated on the basis of this t-test.) Machine limitations set 160 as the maximum possible number of particles allowable in our simulations. As such, ϕ was varied by changing the sphere radius in the respective fixed-size parallel plate and cylindrical cells, while keeping the number of particles fixed at 160.

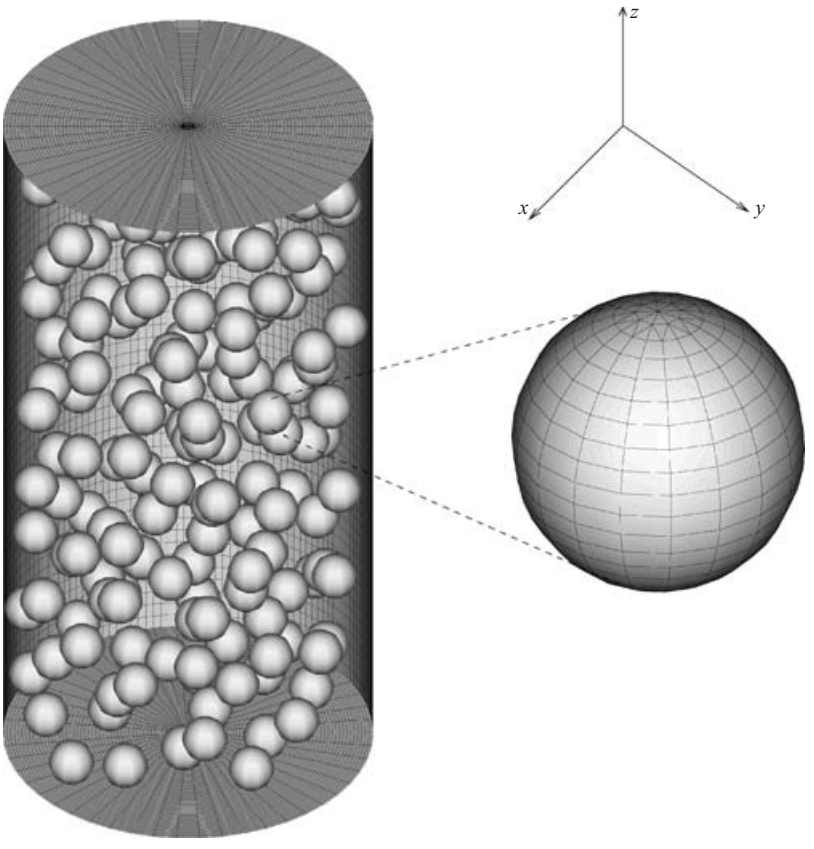

FIGURE 1. A three-dimensional BEM mesh of spherical particles in a tube of radius R and length $4R$ for the case $\phi = 0.10$. The front wall mesh has been cut away in order to view the particles clearly. There are 160 particles in this simulation, with 48 elements on each sphere. Moreover, there are 1600 elements on the cylinder boundaries. The figure was generated via a $Tecplot^{TM}$ that uses lines to connect the nodes. Our simulation used super-parametric elements with quadratic curves to connect the nodes. In order to smooth the geometry of the ball, which is more representative of the actual geometry in our simulation, a 200-element ball mesh was used in drawing this figure.

In both classes of flows, in addition to the prescribed angular velocities $\boldsymbol{\Omega}^i$ on each sphere and the periodic boundary conditions, no-slip boundary conditions were applied at the surfaces of both the particles and walls, while the spheres were rendered net force free. In the shear flow case the lower plate was maintained at rest, while the upper plate was rendered force free at each point, thus allowing it to move with a velocity U determined by the no-slip condition maintained thereon. (The local force-free condition on the upper plate automatically rendered the entire lower plate net-force free.) In the Poiseuille flow case, a no-slip condition was imposed at each point on the cylinder walls, with all velocities being measured relative to these walls. At the same time, a condition of no net force was imposed on the two end caps, thus ensuring that no net force acted on the cylinder walls, in turn ensuring satisfaction of the suspension-scale condition $P = 0$.

An elementary benchmark test of the general BEM scheme involved comparing the BEM-calculated couple G required to cause a single sphere to rotate with an angular

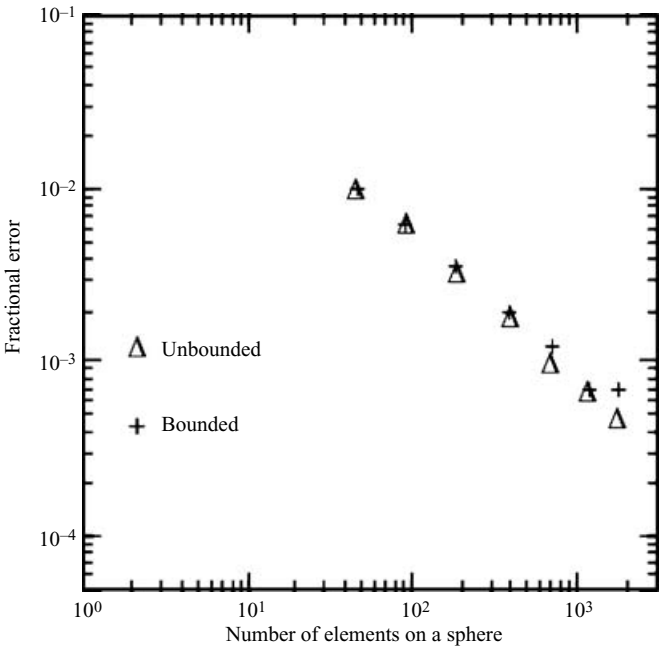

FIGURE 2. Fractional error, $|G - G^\star| / G^\star$, in the couple G on a rotating sphere relative to the theoretical Kirchhoff's law couple, $G^\star$. Results are shown for the respective cases of a single particle rotating in an unbounded fluid and at the centre of a cylindrical tube of radius $R = 10a$. In the latter bounded case, 1600 elements were used on the cylinder boundaries. The number of elements on the sphere varied from 48 to 1800. Note that the effect of the cylindrical boundary upon the couple is less than 0.1 %.

velocity Ω in the effectively unbounded interstitial fluid, otherwise at rest, against Kirchhoff's theoretical value (Happel & Brenner 1965), $G^\star = 8\pi\mu_0 a^3 \Omega$. Figure 2 shows that the calculations converged monotonically with increasing mesh density on the sphere. Explicitly, a less than 1% error in the ratio $|G - G^\star| / G^\star$ resulted from use of 50 mesh elements on the sphere (and 720 elements on the cylinder walls), with 50 being the number of elements later used for each sphere in the multi-sphere simulations of the suspension. Detailed calculations (Feng 2003) revealed that with 48 meshes on each sphere the accuracy of the BEM scheme would prove satisfactory as long as the gap between neighbouring particles was greater than $0.1a$. This restriction places an upper limit of $\phi_{\max} = 0.50$ on the maximum allowable concentration in the case where the spheres are uniformly distant from each other. However, since this uniform spacing condition is not met in random arrangements, we limited ourselves to the concentration range $0 \leqslant \phi \leqslant 0.30$, for which the differences in the simulation results were found to be small at the highest concentration (Feng 2003).

According to the simple shear flow analysis outlined in § 2.1, applying couples to the individual spheres presumably generates the suspension-scale linear velocity profile $v = U(y + H)/2H$. By *presumably* we mean to the extent that the constitutive equations (1.7) and (1.8) are valid. As shown in figure 3, numerical simulation agrees well with theoretical predictions as regards the expected linearity of the suspension-scale velocity profile, which represents the local volume average of the interstitial velocity field. Thus, the simulation implicitly supports the constitutive hypotheses entering into the analysis. In the comparable Poiseuille-like parabolic velocity field

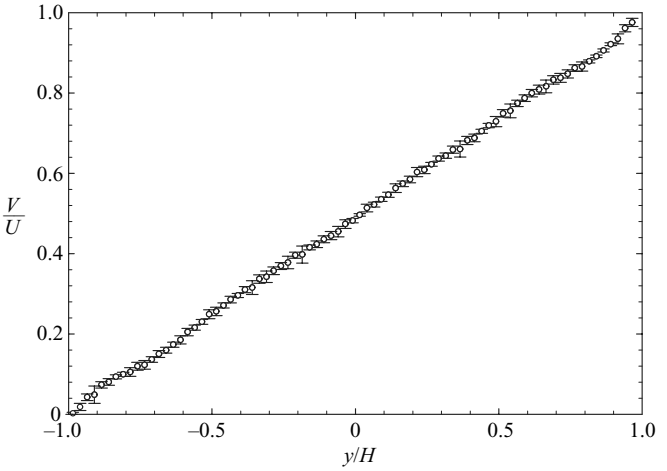

FIGURE 3. Local volume-average velocity field for the Couette-flow case generated by position-independent spins of the spheres bounded by two parallel plates. The result averaged over 30 configurations of 60 particles at $\phi = 0.22$ is shown. If the suspension-scale constitutive equations (1.6) and (1.7) are correct, the hypothetical velocity field would be represented by a straight line connecting the end points. The slight deviation from linearity seen near these two end points is presumably a manifestation of wall effects on those spheres nearest to the two plates.

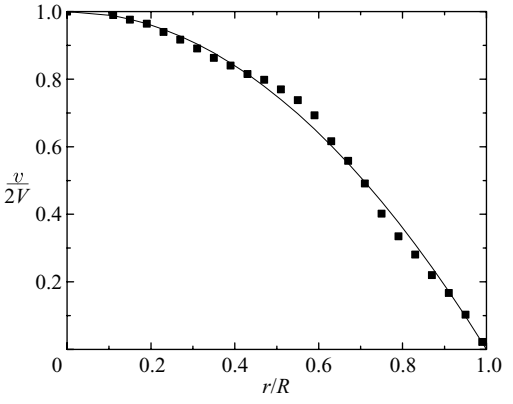

FIGURE 4. Local volume-average velocity field for the Poiseuille-flow case generated by linearly varying spin rates of the spheres within a circular cylindrical tube. No pressure gradient has been applied to the suspension. Results are shown for one configuration at $\phi = 0.22$ using 160 particles. The curve shows the parabolic velocity profile that would be expected were the constitutive equations (1.6) and (1.7) obeyed.

case, figure 4 further confirms the agreement of our numerical simulation scheme with expectations based upon these same constitutive hypotheses.

As shown in figure 5, BEM calculations of the suspension's vortex viscosity based upon both the Couette and Poiseuille flow experiments agree with the theoretical prediction for dilute suspensions, namely $\mu_v/\mu_0 = 1.5\phi$ (Brenner 1970*a*, *b*). Moreover, in concentrated suspensions these simulation results are also seen to agree excellently with the independent Green's function simulation of Prosperetti *et al.*, according to which $\mu_v/\mu_0 = 1.5\phi/\Omega(\phi)$, where in their notation $\Omega(\phi)$ is the *rotational hindrance*

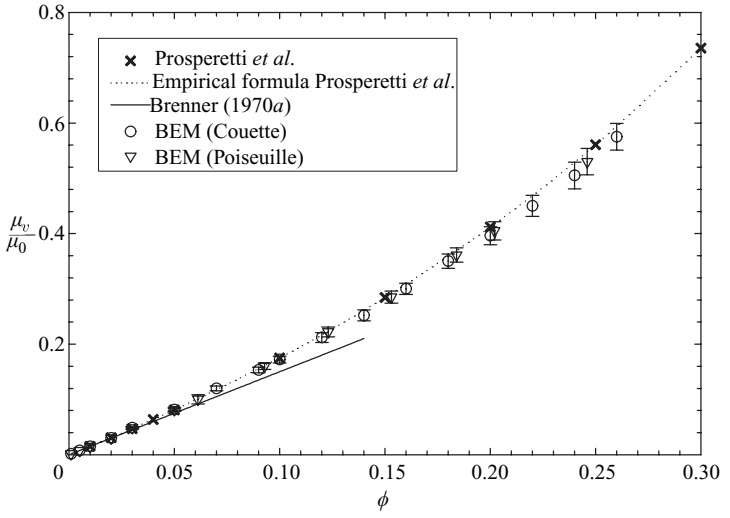

FIGURE 5. Relative vortex viscosity μ_v/μ_0 vs. volume fraction ϕ of suspended spheres obtained from both the Couette- and Poiseuille-flow simulations. The solid line shows the limiting theoretical slope, namely 1.5ϕ in dilute suspensions. Also shown are the Prosperetti *et al.* results.

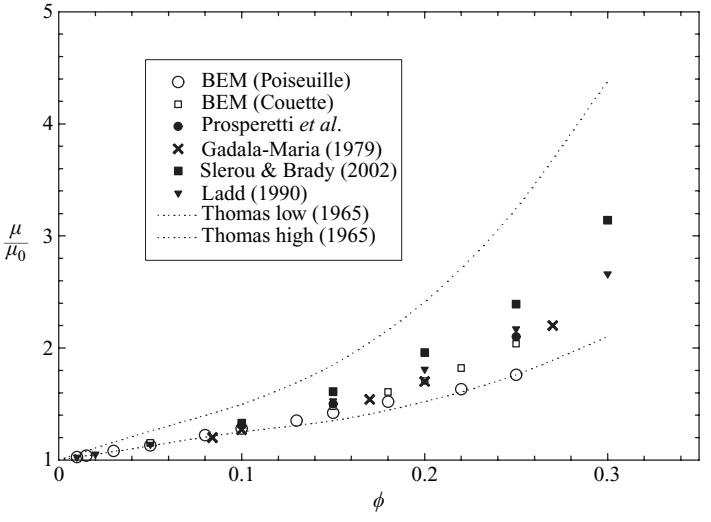

FIGURE 6. Relative shear viscosity μ/μ_0 vs. volume fraction ϕ of suspended spheres obtained from both the Couette- and Poiseuille-flow simulations. Comparison is made with experimental data as well as with the simulation results of others.

function, representing the concentration-dependent correction of the dilute suspension formula. Its functional dependence upon ϕ is presented graphically by those authors up to $\phi = 0.5$, as well as by the empirical curve-fitting formula $\Omega(\phi) = (1-\phi)^{1.5-0.41\phi}$, represented by the dotted line in figure 5.

Having determined the vortex viscosity as outlined above, the corresponding shear viscosity ratio μ/μ_0 vs. ϕ was readily determined from these same BEM data via use of (2.17) in the parallel plate case and (2.30) in the circular tube case. These shear viscosity results are presented in figure 6, again for both Couette and Poiseuille flow kinematics. Also shown for comparison are the (lower and upper bound) experimental

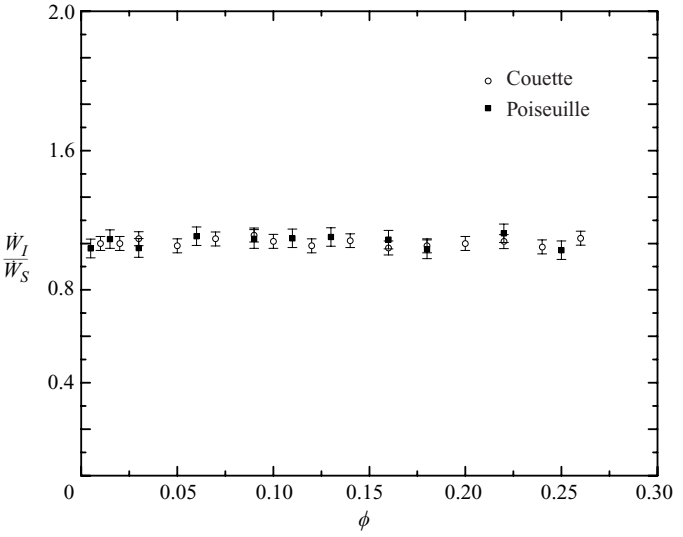

FIGURE 7. Comparison of the respective rate of working ($\dot{W}_I$) at the interstitial scale to that ($\dot{W}_S$) at the suspension scale as a function of particle concentration ϕ for both the Couette- and Poiseuille-flow simulations.

data of Thomas (1965) and the data of Gadala-Maria (1979) as well as the simulation results of a number of other investigators, including Prosperetti *et al.* Obviously, all of these latter simulation results are reasonably consistent with one another as well as with experiment over the entire concentration range displayed. The only issue worthy of more detailed comment is that our Poiseuille flow results were consistently lower than our Couette flow results at the higher concentrations. This appears to be a fundamental shortcoming of the BEM simulation scheme at concentrations above about 25%, where close-contact singularities necessarily become more probable when randomly placing the spheres in the simulation cell. In such circumstances, the simple shear results are more likely to be accurate than the parabolic flow results, since in the former case the close-contact singularity varies like $\ln(1/r)$, whereas it varies like $1/r$ in the latter case, a more severe variation.

As discussed in § 3, scalar energetic arguments may be used in place of the tensor-valued dynamical arguments of § 2 to confirm the validity of (1.7) and (1.8), as well as the correctness of the values of μ and μ_v at the various sphere concentrations. Figure 7 compares the interstitial-scale rate of working $\dot{W}_I$, obtained using the simulation data to effect the summation of (3.2), with the corresponding suspension-scale energy dissipation rate $\dot{W}_S$ derived from (3.1) (as explicitly set forth in (3.3) and (3.5)) by using the dynamically derived μ and μ_v values. That these two independent work-rate calculations agree within acceptable statistical uncertainties, as shown in figure 7, offers evidence of the consistency of our discrete interstitial-scale simulation results with those stemming from our suspension-scale continuum theory analysis. In turn, this agreement further affirms the likely correctness of the constitutive equations (1.7) and (1.8), as well as of the respective vortex and shear viscosity values reported here.

5. Summary and conclusions

Based upon use of BEM simulations, our analysis supports the correctness of the constitutive equation (1.8) for the antisymmetric stress in incompressible suspensions

of randomly dispersed, non-colloidal, force-free spherical particles. As an incidental by-product, for this same class of suspensions our results reaffirm the applicability of Newton's constitutive law, (1.7), for the symmetric portion of the deviatoric stress. During the course of confirming these two constitutive relations, numerical data have been obtained for the respective phenomenological coefficients appearing therein, furnishing information on the dependence of the suspension's vortex and shear viscosities upon the fractional volumetric concentration ϕ of suspended particles, covering the range $0 \leqslant \phi \leqslant 0.30$. In the dilute region, these simulation-derived viscosity-concentration results for the suspension's vortex viscosity agreed well with theoretical expectations (Brenner 1970*a*, *b*). At the higher concentrations our calculations agreed excellently with those of Prosperetti *et al.* On the other hand, the calculated concentration dependence of the shear viscosity in non-dilute suspensions was found in the Poiseuille flow case to differ slightly from the comparable simulation results of others – all based upon simple shear flow – as well as from our own simple shear simulation calculations. A possible limitation of the BEM scheme in concentrated suspensions was suggested as the source of the disparity.

Apart from this, the functional dependence on particle concentration found for both the vortex and shear viscosities proved to be sensibly independent of the particular kinematical flow scheme adopted for their respective computations, whether based upon Couette- or Poiseuille-like velocity fields. Moreover, the excellent agreement obtained between the respective suspension- and interstitial-scale work rates, $\dot{W}_S$ and $\dot{W}_I$, offers strong evidence of the validity of the constitutive equations (1.7) and (1.8), as well as of the correctness of the values obtained for the vortex and shear viscosities.

Our theoretical generation of suspension-scale fluid motion by the use of externally imposed body couples to create individual particle rotations is similar to that occurring in practice in the case of ferrofluids (Rosensweig 1997, 2003), where such couples arise from the action of rotating magnetic fields on suspensions of permanently magnetized particles. Thus, our theoretical calculations of the vortex viscosity may prove useful in interpreting magnetic fluid experiments. In this ferrofluid context, our demonstration in the Appendix that spin-viscosity effects (cf. (A 3)) associated with couple stresses contribute negligibly to the antisymmetric stresses when compared with vortex viscosity contributions suggests the need for caution in attempting to invoke couple stresses when rationalizing experimental magnetic fluid phenomena (Rosensweig 1997, 2003; Rinaldi & Zahn 2002). In this couple-stress context, the long-standing (and as yet unresolved) question of whether the spin boundary condition on solid surfaces should be one of no-slip of the spin field relative to half the vorticity, or otherwise, becomes moot in circumstances where the couple stress vanishes. This is a consequence of the fact that the order of the partial differential equations involving the velocity field (and, hence, the number and type of boundary conditions that need to be specified in order that the velocity and spin fields each be unique) depends upon whether couple stresses are, or are not, present. When absent, as in present circumstances, it is unnecessary to specify suspension-scale spin boundary conditions on solid surfaces.

The authors would like to thank Professors Richard M. Christian and Marc S. Ingber for thoughtful discussions. We are also grateful to Drs David Chaffin and Sam Subia for their help with the numerical modeling, as well as to Dr Patrick T. Reardon for his assistance with the manuscript preparation. Support for this work was provided by the US Department of Energy, Division of Chemical Sciences, Geosciences and Biosciences, Office of Basic Energy Science, US Department of Energy, as well as

by the Environmental Projects Division, National Energy Technology Laboratory and the Advanced Research Program of the Texas Higher Education Coordinating Board.

Appendix. Proof of the vanishing of the couple-stress contribution

In order that a suspension qualify as a continuum, it must satisfy the inequality $l/L \ll 1$, where L is the length scale on which the velocity field varies and $l = O(a/\phi^{1/3})$ is the mean distance between the centres of the suspended spheres, whose radius is a. Typically, the characteristic length L denotes some linear dimension of the apparatus through which the suspension flows, namely $2H$ in our Couette flow case or R in the Poiseuille flow case. Since $a \leqslant l/2$, it follows, irrespective of the value of ϕ, that qualification as a continuum requires that

$$\epsilon \equiv \frac{a}{L} \ll 1, \tag{A 1}$$

an obviously necessary requirement.

When couple stresses are included in the analysis, the angular momentum equation (1.4) is replaced by the expression (Condiff & Dahler 1964)

$$\rho\kappa^2 \frac{\mathrm{D}\boldsymbol{\Omega}}{\mathrm{D}t} = \boldsymbol{\nabla}\cdot\boldsymbol{C} + \boldsymbol{T}_\times + \boldsymbol{G}, \tag{A 2}$$

whereas (1.3) remains unchanged. By analogy with the comparable Newtonian fluid constitutive equation (1.7) for the symmetric portion of the deviatoric stress (including dilatation), Condiff & Dahler (1964) proposed the following constitutive equation for the couple stress (which they supposed to be symmetric):

$$\boldsymbol{C} = \mu_s\left[\boldsymbol{\nabla\Omega} + (\boldsymbol{\nabla\Omega})^\dagger - \tfrac{2}{3}\boldsymbol{I}\boldsymbol{\nabla}\cdot\boldsymbol{\Omega}\right] + \mu_s'\boldsymbol{I}\boldsymbol{\nabla}\cdot\boldsymbol{\Omega}, \tag{A 3}$$

in which μ_s is the spin viscosity and μ_s' the corresponding bulk spin viscosity. Note for both the Couette and Poiseuille flows treated in the present paper that $\boldsymbol{\nabla}\cdot\boldsymbol{\Omega} = 0$, so that the issue of the bulk spin viscosity becomes moot.

Each of these spin-viscosity coefficients is assumed to be a amaterial property of the suspension, and hence a composite property dependent upon the respective material properties of the interstitial fluid and suspended spheres, with the latter assumed in our analysis to interact only hydrodynamically (but not, say, through the mechanism of interparticle colloidal forces, which would introduce additional parameters into the subsequent dimensional analysis). As such, on dimensional grounds, μ_s must be of the functional form

$$\mu_s = a^2\mu_0 f(\phi) \tag{A 4}$$

independently of the density ρ, the only other intrinsic material property upon which it would appear that μ_s could possibly depend. A similar expression applies for μ_s'. Here, $f_s(\phi)$ and $f_s'(\phi)$ are non-dimensional functions of ϕ, which functions we suppose to be of $O(1)$ for all of the particle concentrations studied in this paper. (In dilute systems, f must certainly go to a zero with ϕ, since at $\phi = 0$ the suspension's properties must reduce to those of the interstitial Newtonian fluid, whose state of stress is purely symmetric.) The spin viscosity appearing in (A 4) differs in its dimensions from both the suspension's shear and vortex viscosities, μ and μ_v, which are each necessarily of the respective forms $\mu_0 f(\phi)$ and $\mu_0 f_v(\phi)$, thereby lacking the particle-size a^2 term characterizing the respective spin viscosities. It is this difference which will be seen to account for the failure of the couple stress $\boldsymbol{C}$ to contribute to the physics of the

present class of flow problems relative to the viscous contributions embodied in the deviatoric stress $\boldsymbol{T}$.

In addition to L, a, μ_0 and ϕ, for a given inertia-free interstitial creeping flow the only other independent characteristic suspension-scale parameter serving to determine the scaling of the various fields arising in our force- and pressure-gradient-free, no-slip analysis is the characteristic angular velocity Ω of the suspended spheres. It is the existence of this quantity alone that gives rise to the fluid motion, thus causing the velocity, pressure, stresses, forces and couples to be other than zero in our present class of problems. Thus, each of these suspension-scale continuum quantities must necessarily vanish with Ω, and hence each must be directly proportional to Ω as a consequence of the linearity of the creeping flow equations and the homogeneity of the no-slip, no-force, interstitial boundary conditions. Accordingly, we introduce the following scales for these several fields, in which the variables with a caret represent non-dimensional and scaled, $O(1)$, variables at the suspension scale (from which we have omitted possible multiples involving functions of ϕ):

$$\left.\begin{aligned} &\nabla = L^{-1}\hat{\nabla}, \quad \boldsymbol{\Omega} = \Omega\hat{\boldsymbol{\Omega}}, \quad \boldsymbol{v} = \Omega L\hat{\boldsymbol{v}}, \quad (\boldsymbol{T}^s, \boldsymbol{T}^a) = \mu_0\Omega(\hat{\boldsymbol{T}}^s, \hat{\boldsymbol{T}}^a), \\ &p = \mu_0\Omega\hat{p}, \quad \boldsymbol{C} = a^2L^{-1}\mu_0\Omega\hat{\boldsymbol{C}}, \quad \kappa = a\hat{\kappa}, \quad t = \omega^{-1}\hat{t}. \end{aligned}\right\} \tag{A 5}$$

Introduce these non-dimensional quantities into (1.3) and (A 2), and define the suspension-scale Reynolds number $Re = \Omega L^2\rho/\mu_0$ as well as the scaled material derivative, $\mathrm{D}/\mathrm{D}t = \Omega\hat{\mathrm{D}}/\hat{\mathrm{D}}\hat{t}$, so as to obtain the following scaled linear and angular momentum equations:

$$Re\frac{\hat{\mathrm{D}}\hat{\boldsymbol{v}}}{\hat{\mathrm{D}}\hat{t}} = -\hat{\nabla}\hat{p} + \hat{\nabla}\cdot\hat{\boldsymbol{T}}^s - \tfrac{1}{2}\hat{\nabla}\times\hat{\boldsymbol{T}}_\times \tag{A 6}$$

and

$$\epsilon Re\hat{\kappa}^2\frac{\hat{\mathrm{D}}\hat{\boldsymbol{\Omega}}}{\hat{\mathrm{D}}\hat{t}} = \epsilon\hat{\nabla}\cdot\hat{\boldsymbol{C}} + \hat{\boldsymbol{T}}_\times + \hat{\boldsymbol{G}}. \tag{A 7}$$

In the continuum limit, namely where $\epsilon \to 0$, it follows that the angular momentum equation (A 7) reverts to the (dimensional) couple-stress-free and inertia-free form, $\boldsymbol{T}_\times + \boldsymbol{G} = \boldsymbol{0}$, of (1.4). Moreover, it does so independently of the magnitude of the Reynolds number, in contrast to the comparable behaviour of the inertia term in the linear momentum equation (A 6) and, hence, (1.3).

The preceding purely theoretical arguments regarding the vanishing of the couple stress $\boldsymbol{C}$ are reinforced by our detailed simulation computations for the present class of problems. Thus, if (A 2) and (A 3) were used instead of (1.4) (without the inertial terms), the suspension-scale rate of working $\dot{W}_S$ given by (3.1) would then adopt the form (Brenner & Nadim 1996, Feng 2003)

$$\dot{W}_S = \frac{1}{2\mu}\int_V \boldsymbol{T}^s\!:\!\boldsymbol{T}^s\,\mathrm{d}V + \frac{1}{4\mu_v}\int_V \boldsymbol{T}_\times\cdot\boldsymbol{T}_\times\,\mathrm{d}V + \frac{1}{2\mu_s}\int_V \boldsymbol{C}\!:\!\boldsymbol{C}\,\mathrm{d}V. \tag{A 8}$$

However, the interstitial-scale formula (3.2) for the work rate $\dot{W}_I$ would not change. Consequently, (3.5) for the rate of working in the Poiseuille-flow case would become (Feng 2003)

$$\frac{\dot{W}_s}{V} = \frac{8\mu\bar{V}^2}{R^2}\left[1 + \frac{\mu_v}{\mu}\left(\frac{\Omega R}{2\bar{V}} - 1\right)^2 + \frac{\mu_s}{4\mu}\left(\frac{\Omega}{\bar{V}}\right)^2\right]. \tag{A 9}$$

As such, the presence in (A 9) of any value of μ_s measurably different from zero, stemming from our numerical simulation, would result in a ratio of $\dot{W}_I$ to $\dot{W}_S$ calculated by use of (3.5) differing from unity in figure 7. The fact that our simulations yielded $\dot{W}_I/\dot{W}_S \simeq 1$ thus provides strong confirmation that, for the class of problems studied in this paper, couple stresses do not contribute to suspension-scale continuum phenomena.

REFERENCES

Batchelor, G. K. 1967 *An Introduction to Fluid Dynamics*. Cambridge University Press.

Batchelor, G. K. 1970 The stress system in a suspension of force-free particles. *J. Fluid Mech.* **41**, 545–570.

Brebbia, C. A., Telles, J. C. F. & Wrobel, L. C. 1984 *Boundary Element Techniques*. Springer.

Brenner, H. 1958 Dissipation of energy due to solid particles suspended in a viscous liquid. *Phys. Fluids* **1**, 338–346.

Brenner, H. 1970*a* Rheology of a dilute suspension of dipolar spherical particles in an external field. *J. Colloid Interface Sci.* **32**, 141–158.

Brenner, H. 1970*b* Rheology of two-phase systems. *Annu. Rev. Fluid Mech.* **2**, 137–176.

Brenner, H. 1984 Antisymmetric stresses induced by the rigid-body rotation of dipolar suspensions – Vortex flow. *Intl J. Engng Sci.* **22**, 645–682.

Brenner, H. & Nadim, A. 1996 The Lorentz reciprocal theorem for micropolar fluids. *J. Engng Maths* **30**, 169–176.

Brenner, H. & Weissman, M. H. 1972 Rheology of a dilute suspension of dipolar spherical particles in an external field: II. Effects of rotary Brownian motion. *J. Colloid Interface Sci.* **41**, 499–531 (l972).

Burgers, J. M. 1938 *Second Report on Viscosity and Plasticity*. Verh. KNAW Afd. Natuuurkunde.

Condiff, D. W. & Dahler, J. S. 1964 Fluid mechanical aspects of antisymmetric stress. *Phys. Fluids* **69**, 842–854.

Cox, R. G. & Brenner, H. 1971 The rheology of a suspension in a Newtonian fluid. *Chem. Engng Sci.* **26**, 65–93.

Dahler, J. S. & Scriven, L. E. 1961 Angular momentum of continua. *Nature* **192**, 36–37.

Dingman, S. E. 1992 Three-dimensional simulation of fluid-particle interactions using the boundary element method. PhD thesis, University of New Mexico.

Drazer, G., Koplik, J., Khusid, B. & Acrivos, A. 2004 Fluid mechanical aspects of antisymmetric stress. Microstructure and velocity fluctuations in sheared suspensions. *J. Fluid Mech.* **511**, 237–263.

Einstein, A. 1956 *Investigations on the Theory of the Brownian Movement*. Dover.

Falade, A. & Brenner, H. 1988 First-order curvature effects upon the Stokes resistance of a spherical particle moving in close proximity to a solid wall. *J. Fluid Mech.* **193**, 533–568.

Feng, S. 2003 Coupling of linear and angular momentum in concentrated suspensions of spheres. PhD thesis, Texas Tech University.

Gadala-Maria, F. 1979 The rheology of concentrated suspensions. PhD thesis, Stanford University.

Goldman, A. J., Cox, R. G. & Brenner, H. 1967 Slow viscous motion of a sphere parallel to a plane wall. Part II. Couette. *Chem. Engng Sci.* **22**, 653–660.

de Groot, S. & Mazur, P. 1962 *Non-equilibrium Thermodynamics*. Interscience.

Happel, J. & Brenner, H. 1965 *Low Reynolds Number Hydrodynamics*. Prentice-Hall.

Ichicki, K. & Prosperetti, A. 1994 Faxen-like relations for a nonuniform suspension. *Phys. Fluids* **16**, 2483–2497.

Ingber, M. S. 1989 Numerical simulation of the hydrodynamic interaction between a sedimenting particle and a neutrally buoyant particle. *Intl J. Numer. Meth. Fluids* **9**, 263–273.

Johnson, R. A. 1965 *Probability and Statistics for Engineers*. Prentice Hall.

Kim, S. & Karrila, S. J. 1991 *Microhydrodynamics: Principles and Selected Applications*. Butterworth-Heinemann.

Ladd, A. J. C. 1990 Hydrodynamic transport coefficients of random dispersions of hard spheres. *J. Chem. Phys.* **93**, 3484–3494.

Landau, L. D. & Lifschitz, E. M. 1959 *Fluid Mechanics*. Oxford.

Marchioro, M., Tanksley, M. & Prosperetti, A. 2000 Flow of spatially non-uniform suspensions – Part I: Phenomenology. *Intl J. Multiphase Flow* **26**, 783–831.

Marchioro, M., Tanksley, M., Wang, W. & Prosperetti, A. 2001 Flow of spatially non-uniform suspensions – Part II: Systematic derivation of closure relations. *Intl J. Multiphase Flow* **27**, 237–276.

Mondy, L. A., Ingber, M. S. & Dingman, S. E. 1991 Boundary element method simulations of a ball falling through quiescent suspensions. *J. Rheol.* **35**, 825–848.

Rinaldi, C. & Brenner, H. 2002 Body versus surface forces in continuum mechanics: Is the Maxwell stress tensor a physically objective Cauchy stress? *Phys. Rev.* E **65**, 36615.

Rinaldi, C. & Zahn, M. 2002 Effects of spin viscosity on ferrofluid flow profiles in alternating and rotating magnetic fields. *Phys. Fluids* **14**, 2847–2870.

Rosensweig, R. E. 1997 *Ferrohydynamics*. Dover.

Rosensweig, R. E. 2003 *Basic Equations for Magnetic Fluids with Internal Rotations*. Lecture Notes in Physics. Vol. **594**, pp. 61–84. Springer.

Sierou, A. & Brady, J. F. 2002 Rheology and microstructure in concentrated noncolloidal suspensions. *J. Rheol.* **46**, 1031–1056.

Thomas, D. G 1969 Transport characteristics of suspensions: VII A note on the viscosity of Newtonian suspensions of uniform spherical particles. *J. Colloid Sci.* **20**, 267–277.

Wang, W. & Prosperetti, A. 2001 Flow of spatially non-uniform suspensions – Part III: Closure relations for porous media and spinning particles. *Intl J. Multiphase Flow* **27**, 1627–1653.

Zuzovsky, M., Adler P. M. & Brenner, H. 1984 Spatially periodic suspensions of convex particles in linear shear flows. III. Dilute arrays of spheres suspended in Newtonian fluids. *Phys. Fluids* **26**, 1714–1721.